THE ASTROPHYSICAL JOURNAL, 404:328–332, 1993 February 10

SPATIALLY RESOLVED SPECTRA OF SILICATE DUST AROUND α ORIONIS[1]

G. C. SLOAN[2]
Department of Physics and Astronomy, University of Wyoming, P.O. Box 3905, Laramie, WY 82071
G. L. GRASDALEN
G-star Enterprises, 286 South Pennsylvania, Denver, CO 80209
AND
PAUL D. LEVAN[3]
Phillips Laboratory, PL/GPOB, Hanscom AFB, MA 01731
Received 1992 April 13; accepted 1992 July 23

ABSTRACT

We have observed α Orionis with a 10 μm long-slit spectrometer. By applying maximum entropy reconstruction techniques, we have spatially resolved the silicate emission from the circumstellar shell. The emissivity derived from our silicate spectrum compares favorably with published emissivity profiles describing circumstellar silicates. The lack of silicate emission in the direction of the central star suggests that the circumstellar dust may not be distributed in a spherical shell.

Subject headings: circumstellar matter — dust, extinction — infrared: stars — stars: individual (α Orionis)

1. INTRODUCTION

The star α Orionis has become the quintessential case of an evolved star with a circumstellar shell. Expanding material around α Ori was first identified by Adams & MacCormack (1935), who detected blueshifted absorption cores in the H, K, D, and Al I and II lines in spectra of α Ori. Deutsch (1956) clarified the situation when he described similar spectral properties in α Her. In this system, he argued that the absorption lines seen in the spectra of both visual components arose in an extended circumstellar envelope. He identified several additional stars, including α Ori, which also possessed circumstellar envelopes and attributed these to mass-loss from the central star. Early infrared observations provided clues to the nature of the material around α Ori by revealing emission features from silicate dust at 10 and 20 μm (Gillett, Low, & Stein 1968; Woolf & Ney 1969).

Since McCarthy, Low, & Howell (1977) first resolved the dust shell, further interferometric work has substantially improved our understanding of α Ori and its shell. Bester et al. (1991) used heterodyne interferometry at 11 μm to resolve the shell around α Ori. They combined their data with earlier speckle observations by Sutton (1979) and Howell, McCarthy, & Low (1981), and modeled the resulting visibility curve with an optically thin ($\tau = 0.042$) hollow dust shell with an inner radius of 0.″9 ($\sim 40 R_*$). Dyck & Benson (1992) modeled their speckle observations from 8 to 13 μm with a Gaussian with a full width at half maximum (FWHM) of 2.″6. We compared the visibility curve of their model with that of Bester et al. and found that the two agree very closely.

Bester et al. (1991) argued that the large inner radius of the dust shell and its low dust temperature (280 K) make it unlikely that the inner edge of the shell corresponds to the condensation radius of the dust. Rather, α Ori has ended its most recent mass loss phase. Dust is no longer condensing, and the inner boundary of the shell is moving away from the star. In this scenario, the grains around α Ori are still young. Assuming a distance of 200 pc and a constant velocity of 10 km s^{-1} (Weymann 1962), the material presently located 0.″9 from the central star would be about 85 yr old.

We chose to study α Ori with an infrared slit spectrometer because of its high infrared brightness and because the recent interferometric results of Bester et al. (1991) and Dyck & Benson (1992) indicated that we could spatially resolve emission from its dust shell.

2. OBSERVATIONS

We observed α Ori on 1991 February 6 with GLADYS, the Geophysics Laboratory 10 μm array spectrometer (LeVan 1990), mounted on the 2.3 m telescope at the Wyoming Infrared Observatory (WIRO). After integrating on α Ori, we immediately observed α Tau to provide both a spectral and point source reference observed at nearly the same air mass, direction in the sky, and time.

For both objects, the slit and the chop throw were in the north/south direction. We chopped at a frequency of 1.5 Hz, using the three-beam chop described by Landau, Grasdalen, & Sloan (1992). For α Ori, we took 10 images, each consisting of 40 chops, and for α Tau, 20 images of 120 chops each. We allowed the objects to slowly drift along the slit, so that the position of the star in the slit would shift slightly from one image to the next. Further details of our observing procedure are described in Grasdalen, Sloan, & LeVan (1992, hereafter Paper I).

3. DATA REDUCTION AND ANALYSIS

We determined our wavelength calibration as described by LeVan (1990) and flat-fielded our data as described in Paper I. In Paper I, we presented a spatiogram (plot of width vs. wavelength) for our α Ori data, which demonstrated that we had resolved emission from silicate dust around α Ori.

We extracted a one-dimensional spectrum from each two-dimensional image of α Ori and co-added the resulting spectra to produce the spectrum in Figure 1. We corrected for atmo-

[1] Contribution 136 of the Wyoming Infrared Observatory.
[2] Postal address: Phillips Laboratory, PL/GPOB, Hanscom AFB, MA 01731.
[3] Postal address: Phillips Laboratory, PL/VTRP, Kirtland AFB, NM 87117.

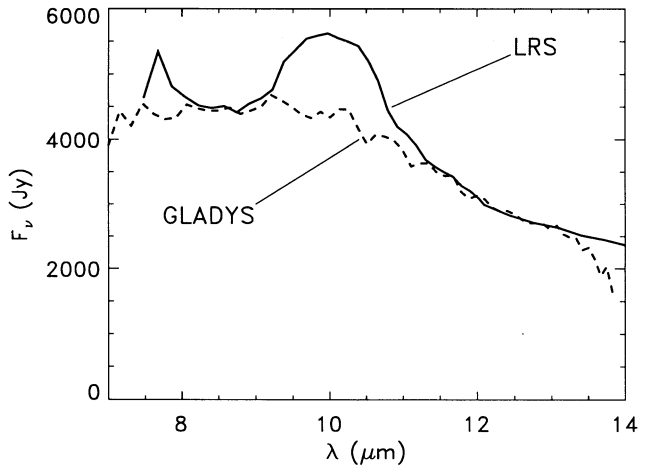

FIG. 1.—Spectra of α Ori from the LRS and GLADYS. The LRS spectrum contains much more silicate emission than seen by GLADYS, indicating that the emitting region is larger than the 2″ × 9″ slit in GLADYS. The higher noise in the GLADYS spectrum is primarily the result of an insufficient integration time of the spectral standard, α Tau.

spheric and instrumental transmission and detector response by dividing by α Tau and then multiplying by a λ^{-2} Rayleigh-Jeans distribution. Figure 1 illustrates the lack of silicate emission observed by GLADYS when compared to results from the *IRAS* Low Resolution Spectrometer (LRS). This difference strongly supports the notion that the shell around α Ori is extended on the order of at least a few arcsec. *Much of the silicate emission arises in a region outside the 2″ × 9″ slit used by GLADYS.*

In order to learn more about the nature of the extended emission, we applied maximum entropy techniques to our α Ori data to remove the effects of atmospheric seeing as well as diffraction from the telescope and instrument. Maximum entropy reconstruction solves a number of difficulties with the reduction of long-slit spectroscopic data. Presently, GLADYS uses an array of Si:Ga detectors in a 10 × 62 pixel configuration. The pixel size (0.″88) is closely matched to the diffraction limit of the telescope (1.″0), so each individual image is spatially undersampled. The dispersion axis of the NaCl prism is inclined slightly to the long array axis. In addition, lines of constant wavelength are not orthogonal to the dispersion axis or to either of the array axes. Geometric transformations to orthogonalize the data would reduce spatial and spectral resolution, since they require interpolation in our undersampled array. Co-adding the individual data images would require a shift-and-add algorithm, which again would reduce the resolution.

Our reconstruction method is based on the MEMSYS algorithm of Gull & Skilling (1984, 1989). We chose to map the original 10 row data into 19 rows, each 0.″44 in extent. The key to implementing a maximum entropy algorithm is to adequately describe the behavior of the point spread function (PSF). The PSF is the result of the seeing disk from the atmosphere, the Airy disk from the telescope, and the diffraction pattern from the instrument, each of which is a function of wavelength, as well as the motion of the star within the slit.

To analytically describe the function PSF(λ) precisely would be impossible. A complete description of the full PSF in both the spatial and spectral directions would require observations of monochromatic point sources. We have chosen only to correct for the effects of the PSF in the spatial direction, determining a one-dimensional PSF at each wavelength instead of a full, two-dimensional PSF.

We found the best approach was to model the PSF at each wavelength with the sum of a Gaussian and an exponential, using our 20 images of α Tau as a point source reference. A Gaussian alone is inadequate for MEMSYS, since it underestimates the wings of the PSF.

The first step in our procedure was to determine the position of α Tau in the slit in each image. At each wavelength, we fit a Gaussian to the spatial cut to determine the fractional pixel position of the center of the PSF. As explained above, these positions fall on a line slightly inclined to the 62 pixel axis of the array. We used a least-squares method to determine the position of this line on our array, and thus the precise position of the star in our slit in each image.

Since α Tau slowly drifted during our integration, we actually have 20 values across each pixel, one from each image. The net effect is that we have heavily oversampled the PSF spatially. We generated PSF profiles at each wavelength by plotting data from all 20 images, shifted by their respective offsets. We fit our Gaussian and exponential model to the data using a downhill simplex method (Press et al. 1988), minimizing the square of the differences between our model and the data. Figure 2 illustrates actual profiles and our models fit to them at two wavelengths. We produced a separate PSF(λ) surface for each α Ori image, correcting for the relative positions of α Ori in the slit.

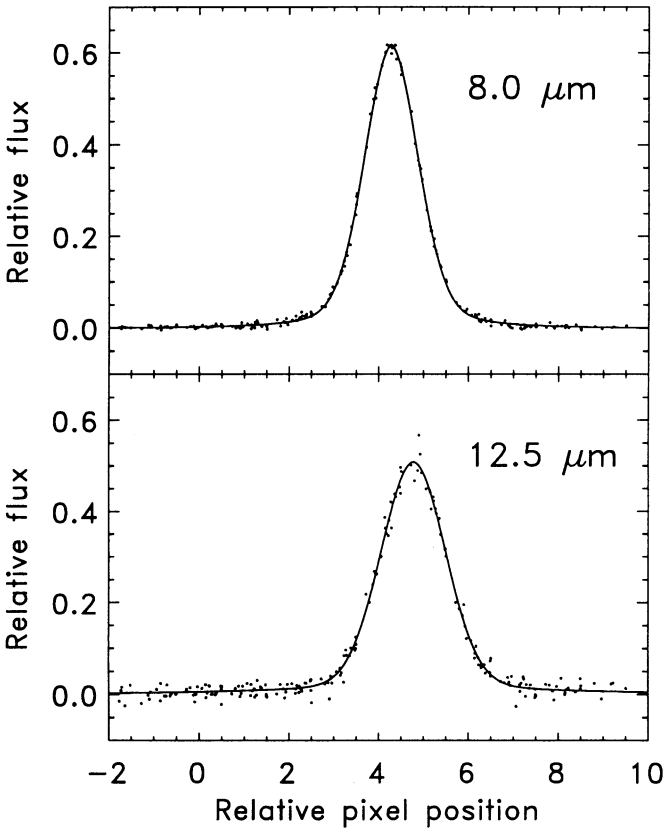

FIG. 2.—Point spread functions based on α Tau data at wavelengths of 8.0 and 12.5 μm. The dots represent the data from 20 individual α Tau images, corrected for the position of the star in the slit. The solid lines are our best fit to the data, using a model profile which is the sum of the Gaussian and an exponential. The PSF is clearly broader at longer wavelengths.

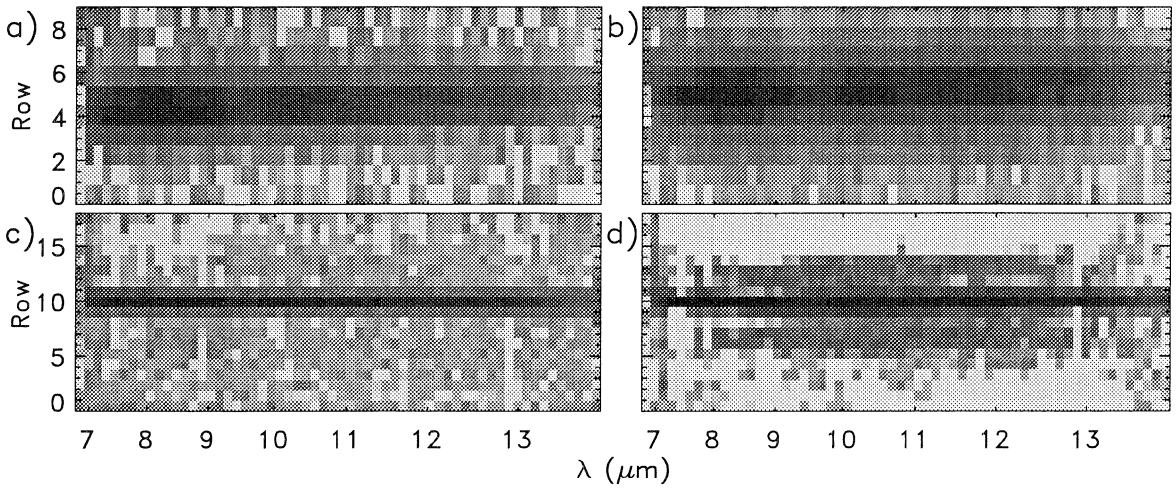

FIG. 3.—Results of MEMSYS maximum entropy reconstruction, illustrated with gray-scale images of the log of the flux. (*a*) A single α Tau image before reconstruction. (*b*) The sum of 20 reconstructed α Tau images. (*c*) A single α Ori image prior to reconstruction. (*d*) The sum of the reconstructed α Ori images. The reconstruction regridded the original 10 row data onto 19 rows and corrected for the angle between the dispersion axis and the array apparent in the upper panels. The reconstruction of α Ori contains emission away from the star well above the noise. The reconstruction of α Tau is nearly a point source.

We tested our MEMSYS algorithm by generating synthetic images of α Tau with side-row spectra. We created two synthetic images, one with side-row spectra spaced one pixel (0.″9) on either side of the central spectrum and reduced in strength by a factor of 10, and the other with side-row spectra spaced 2 pixels (1.″8) away. MEMSYS had no difficulty with the 2″ spacing, resolving the side spectra nicely. The 1″ spacing posed more of a problem. The reconstructions were clearly broader than a point source, but most of the excess emission appeared only 0.″5 away from the central row. These results suggest that MEMSYS systematically shifts low surface brightness emission originating close to the central row even closer.

Figure 3 illustrates the results of our MEMSYS reconstructions of α Tau and α Ori. MEMSYS shifted the center of all α Ori images to row 10, allowing us to co-add them directly; no shifting or interpolating was necessary. We reconstructed the α Tau images to test our algorithm; it is gratifying that the reconstruction of α Tau is very close to that expected for a point source. The reconstruction of α Ori contains emission away from the central star well above the noise level. *We have successfully resolved the dust shell of α Ori!*

4. RESULTS

The profile of the star and shell across our slit illustrated in Figure 4 shows that we have resolved the circumstellar emission from α Ori. As a result, we do not have to make any assumptions about the nature of the stellar flux to isolate the spectral contribution from the shell; we have observed it directly.

We produced a spectrum in Figure 5 of the outer emission regions (rows 5–8 and 12–15 in our reconstruction) by summing over them, dividing by our spectrum of α Tau, and multiplying by the assumed shape of the actual spectrum of α Tau. (We discuss the nature of the actual spectrum of α Tau below.) The resulting spectrum is reasonably smooth, demonstrating the quality of the MEMSYS reconstruction in these

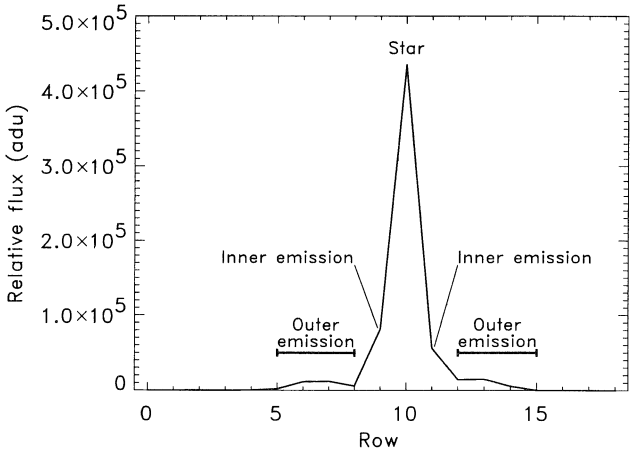

FIG. 4.—Profile of α Ori across our slit, summed from 9 to 12 μm. Each row corresponds to 0.″44. The central row (10) contains the stellar spectrum. The outer silicate emission region (rows 5–8 and 12–15) is underneath the solid bars in the figure. The rows adjacent to the central row (9 and 11) represent the inner silicate emission region.

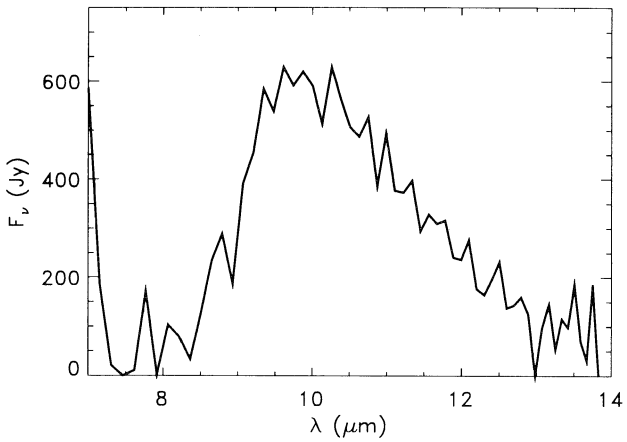

FIG. 5.—Spectrum from the outer emission region (rows 5–8 and 12–15). The spectrum contains only silicate emission.

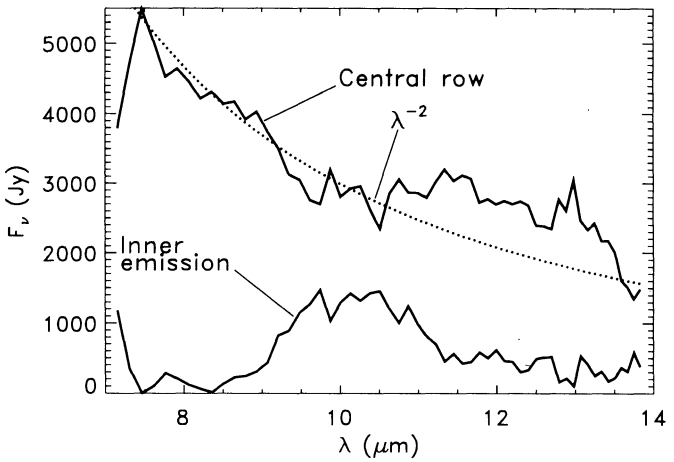

FIG. 6.—Spectra of the central row and the inner emission region of our reconstruction. Most of the noise in the spectra results from difficulties MEMSYS had disentangling the silicate and photospheric emission in this region. The dotted curve is a λ^{-2} Rayleigh-Jeans distribution.

rows. The spectrum is clearly silicate in nature; there is no contamination from the photosphere.

The inner region of silicate emission (rows 9 and 11) is more problematic, primarily because MEMSYS had to dig the silicate emission in these rows out from under the substantial flux from α Ori. Nonetheless, the reconstructed spectrum from this region contains little or no photospheric emission (Fig. 6); it arises from silicate material close to α Ori.

The central row contains no silicate emission at 10 μm (Fig. 6). It is surprising that the emission from this row appears to be photospheric, given that silicate emission appears only 0.″5 to either side. Using our tests with synthetic side-row spectra to interpret these results, we conclude that the inner region producing the silicate emission close to the star in our reconstructions is on the order of 1″ away from α Ori.

At 12 μm, the central spectrum has excess emission, which we attribute to silicates which have not been resolved from the photospheric spectrum. The poorer resolution results from the larger diffraction pattern and lower signal-to-noise ratio at these longer wavelengths. This emission probably arises from the same region producing the inner silicate emission.

5. DISCUSSION

Cohen et al. (1992) have raised the troubling issue that our understanding of photospheric emission from late-type giants in this wavelength regime is much less advanced than we had hoped. In particular, these stars appear to exhibit absorption from SiO in their spectra, including those stars long assumed to have featureless spectra at 10 μm such as α Tau and α Boo. We decided to use their photometrically calibrated spectrum for α Tau (Cohen, Walker, & Witteborn 1992) to calibrate the spectra in Figures 5–7. To calibrate the GLADYS spectrum in Figure 1, however, we used a Rayleigh-Jeans distribution, since we are comparing our data to the LRS data, which were calibrated in a similar manner. For our purposes, the only significant departure in the spectrum of α Tau from a Rayleigh-Jeans distribution is the SiO absorption band around 8 μm. This deviation has little effect on our silicate profiles, since silicate emission is minimal near 8 μm. It does, however, affect the shape of the photospheric spectrum of α Ori in Figure 6.

We are not aware of any M supergiants for which the photospheric spectrum is not veiled by silicate emission. Given our lack of understanding of what the spectrum from the photosphere of α Ori should look like, interpreting the nature of the central spectrum of our reconstructions is very difficult.

A comparison of the silicate emission in Figures 5 and 6 shows that the silicate emission feature from the outer region is broader and peaks at a shorter wavelength than the emission from the inner region. The difference in the width of the features would be eliminated if we included the excess emission around 12 μm seen in the central row with the inner emission. It is tempting to relate the shift in peak wavelength to the evolutionary scenario for silicate grains proposed by Little-Marenin & Little (1990) and Stencel et al. (1990), but given the difficulties in reconstructing the inner rows, we cannot rule out the possibility that this shift is just an artifact of our reconstruction method.

To convert our silicate spectrum to an emissivity profile, we have divided by a blackbody of temperature 280 K. Bester et al. (1991) give a dust temperature at the inner shell boundary of 280 K. We also determined a dust temperature by fitting silicate profiles to the silicate features extracted from the α Ori spectrum taken by the LRS. The temperature varied from 280 to 290 K, depending on the assumed profile.

In Figure 7, we compare the emissivity from the outer silicate emission region with the profiles of Draine & Lee (1984, hereafter DL; tabulated by Draine 1985) and Ossenkopf, Henning, & Mathis (1992, hereafter OHM). The DL profile is significantly broader than ours, but theirs is not a model of circumstellar silicates. Rather, they obtained their profile by matching the shape of the silicate feature seen in the Trapezium, which arises from interstellar silicate grains. The difference between the properties of interstellar and circumstellar silicates has been pointed out before (e.g., Nuth & Hecht 1990; Simpson 1991) and is discussed extensively by OHM. The general shape of the OHM profile matches ours well, although our profile is shifted slightly to the blue. Their profile is based primarily on feature profiles extracted from LRS spectra of evolved stars by Volk & Kwok (1988) and is more representative of circumstellar silicates. We have also compared our profile with the opacity curve given by Dyck & Benson (1992). Their profile is shifted to the red slightly, but has a very similar shape, much like the OHM profile.

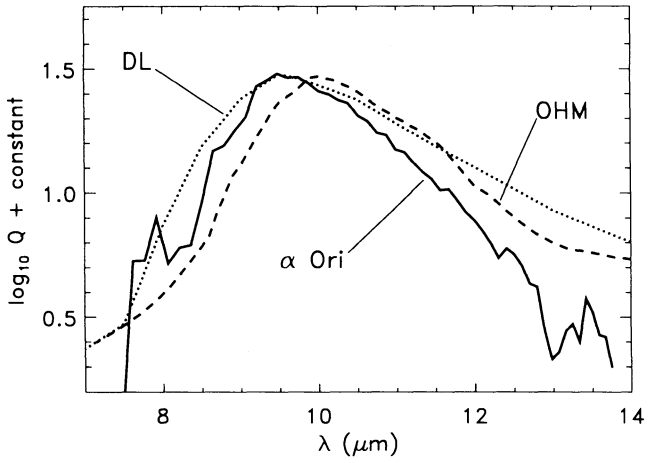

FIG. 7.—Comparison of emissivities of the silicate dust around α Ori with profiles by Ossenkopf et al. (1992, labeled as OHM) and Draine & Lee (1984, labeled as DL). The OHM profile is the dashed line; the dotted line is the DL profile. We produced the α Ori profile by summing only the rows containing the outer emission region, dividing by a 280 K blackbody, and smoothing the result.

Our reconstructions show very little silicate dust along the line of sight (LOS) directly toward α Ori. This result is not consistent with any spherically symmetric shell because in such a model, the LOS must pass through the shell in front of and behind the star. For example, in the hollow shell of Bester et al. (1991), the central row in our reconstructions would contain 95% of the silicate flux in either adjacent row. For any spherically symmetric model, this fraction is still large. There are other geometries which would be consistent with our work and the interferometry results of Bester et al. (1991) and Dyck & Benson (1992). The emission might arise from clumps around α Ori with a characteristic separation of 0".9, or the dust might be distributed in a biconical geometry.

We thank R. Canterna for providing us with computer facilities for data reduction. We used IDL (Interactive Data Language) to reduce and analyze our data and found it to be a wonderful package. The LRS data base at the Center for Astrophysics and Space Astronomy at CU Boulder also proved very useful. It is maintained by R. Stencel, who along with H. M. Dyck and R. Canterna, provided us with helpful discussions and comments. We are also grateful to M. Cohen and F. Witteborn, who furnished us with their corrected spectrum of α Tau, and J. Mathis, who sent us a preliminary version of the manuscript of OHM. Astronomy at WIRO is supported by the State of Wyoming and the Air Force Office of Scientific Research.

REFERENCES

Adams, H. A., & MacCormack, E. 1935, ApJ, 81, 119
Bester, M., Danchi, W. C., Degiacomi, C. G., Townes, C. H., & Geballe, T. R. 1991, ApJ, 367, L27
Cohen, M., Walker, R. G., & Witteborn, F. C. 1992, AJ, in press
Cohen, M., Witteborn, F. C., Carbon, D., Augason, G., Wooden, D., Bregman, J. D., & Goorvitch, D. 1992, AJ, in press
Deutsch, A. J. 1956, ApJ, 123, 210
Draine, B. T. 1985, ApJS, 57, 587
Draine, B. T., & Lee, H. M. 1984, ApJ, 285, 89 (DL)
Dyck, H. M., & Benson, J. A. 1992, AJ, 104, 377
Gillett, F. C., Low, F. J., & Stein, W. A. 1968, ApJ, 154, 677
Grasdalen, G. L., Sloan, G. C., & LeVan, P. D. 1992, ApJ, 384, L25 (Paper I)
Gull S. F., & Skilling, J. 1984, Proc. IEEE, 131, 646
———. 1989, Quantified Maximum Entropy "MEMSYS 3" Users' Manual (London: Maximum Entropy Data Consultants Ltd.)
Howell, R. R., McCarthy, D. W., & Low, F. J. 1981, ApJ, 251, L21
Landau, R., Grasdalen, G., & Sloan, G. C. 1992, A&A, 259, 696
LeVan, P. D. 1990, PASP, 102, 190
Little-Marenin, I. R., & Little, S. J. 1990, AJ, 99, 1173
McCarthy, D. W., Low, F. H., & Howell, R. 1977, ApJ, 214, L85
Nuth III, J. A., & Hecht, J. H., 1990, Ap&SS, 163, 79
Ossenkopf, V., Henning, Th., & Mathis, J. S. 1992, A&A, 261, 567 (OHM)
Press, W. H., Flannery, B. P., Teukolsky, S. A., & Vetterling, W. T. 1988, Numerical Recipes in C: The Art of Scientific Computing (Cambridge: Cambridge Univ. Press)
Simpson, J. P. 1991, ApJ, 368, 570
Stencel, R. E., Nuth III, J. A., Little-Marenin, I. R., & Little, S. J. 1990, ApJ, 350, L45
Sutton, E. C. 1979, in IAU Colloq. 50, High Angular Resolution Stellar Interferometry, ed. J. Davis & W. J. Tango (Sydney: Univ.), 16
Volk, K., & Kwok, S. 1988, ApJ, 331, 435
Weymann, R. 1962, ApJ, 136, 844
Woolf, N. J., & Ney, E. P. 1969, ApJ, 155, L181